Chinese Chemical Letters 34 (2023) 107720

Contents lists available at ScienceDirect

Chinese Chemical Letters

journal homepage: www.elsevier.com/locate/cclet

Effects of polymer molecular weight on *in vitro* and *in vivo* performance of nanoparticle drug carriers for lymphoma therapy

Xinru You[a,b], Liying Wang[b], Junfu Zhang[c], Tong Tong[b], Chunlei Dai[b], Chun Chen[a,*], Jun Wu[a,b,*]

[a] Department of Pediatrics, The Seventh Affiliated Hospital of Sun Yat-sen University, Shenzhen 518107, China
[b] School of Biomedical Engineering, Sun Yat-sen University, Shenzhen 518057, China
[c] Department of Urology, The Seventh Affiliated Hospital of Sun Yat-sen University, Shenzhen 518107, China

ARTICLE INFO

Article history:
Received 14 May 2022
Revised 23 July 2022
Accepted 27 July 2022
Available online 2 August 2022

Keywords:
Nanoparticles
Drug delivery
Lymphoma therapy
Polymer molecular weight
Poly(ester amide)

ABSTRACT

The clinical efficacy of chemotherapeutic drugs is hindered by their poor aqueous solubility, low bioavailability and severe side effects. In recent years, polymeric nanocarriers have been used for drug delivery to improve the efficacy of many chemotherapeutics. In this study, a series of biodegradable phenylalanine-based poly(ester amide) (Phe-PEA) with tunable molecular weights (MWs) were synthesized to systematically investigate the relationship between the polymer MW and the efficacy of the corresponding polymeric nanoparticles (NPs). The results indicated that a range of polymers with different MWs can be obtained by varying the monomer ratio or reaction time. Doxorubicin (DOX), a classic clinical lymphoma treatment strategy, was selected as a model drug. The loading capacity and stability of the higher MW polymeric NPs were superior to those of the lower MW ones. Moreover, *in vitro* and *in vivo* data revealed that high MW polymeric NPs had better anticancer efficacy against lymphoma and higher biosafety than low MW polymeric nanoparticles and DOX. Therefore, this study suggests the importance of polymer MW for drug delivery systems and provides valuable guidance for the design of enhanced polymeric drug carriers for lymphoma treatment.

© 2023 Published by Elsevier B.V. on behalf of Chinese Chemical Society and Institute of Materia Medica, Chinese Academy of Medical Sciences.

In recent decades, cancer has posed a serious threat to human's health owing to its increasing morbidity and mortality rate [1]. Many advanced clinical treatments have been used to fight against tumor such as surgery [2], radiotherapy [3] and chemotherapy [4,5]. Among these, chemotherapy based on cytotoxic drugs is the most common method for cancer treatment. However, the clinical efficacy of chemotherapeutic drugs is hindered by poor aqueous solubility, low bioavailability and severe side effects [4,6,7]. Nanoparticles (NPs) have unique advantages in improving the solubility of hydrophobic drugs, prolonging blood circulation and enhancing drug accumulation in tumor sites, making them promising for cancer treatment [6,8–10]. Polymeric nanocarriers have attracted the interest of researchers owing to their diverse structures, biodegradability, and controllable drug delivery [11–15]. However, the delivery efficacy has aplenty of space for improving by adjusting the properties of the polymers [16–18].

The physical properties, such as molecular weight (MW), solubility and glass transition temperature of degradable polymers, significantly affect the drug delivery properties of polymeric NPs as well as the biological properties of polymeric drug delivery systems [19,20]. Recently, an increasing number of scientists focused on the relationship between the polymer MW and the performance of the corresponding polymeric NPs [21]. For example, Dahlman *et al.* developed a type of polymeric NPs formed by low MW polyamines and lipids for siRNA delivery, which facilitated the simultaneous silencing of multiple genes and mediated the most durable non-liver silencing [22,23]. Furthermore, Li and his coworkers demonstrated that by increasing the MW of developed cationic polymer mucoadhesive NPs, they have prolonged the gene transfer time and improved the penetration through the bladder permeability barrier [24]. Among them, tuning the polymer MW can affect the cellular uptake, circulation time and accumulation ability, which led to significantly enhanced therapeutic efficacy [25,26].

With improved chemical modifications, polymers with controlled MWs can be fabricated [27–29]. In the present study, a series of phenylalanine-based poly(ester amide)s (Phe-PEAs) with precisely controlled structures was established and developed as

* Corresponding authors.
E-mail addresses: chenchun69@126.com (C. Chen), wujun29@mail.sysu.edu.cn (J. Wu).

https://doi.org/10.1016/j.cclet.2022.07.063
1001-8417/© 2023 Published by Elsevier B.V. on behalf of Chinese Chemical Society and Institute of Materia Medica, Chinese Academy of Medical Sciences.

a model polymer library to investigate the effects of the polymer MW on the DOX delivery and lymphoma therapy efficacy. Phe-PEA was synthesized from three building blocks: dial, diol and amino acid. By changing the molar ratio of monomers and reaction time, the polymer MW could be finely tuned. Then, two different MWs (a high MW of 35–45 kDa and a low MW of 6–7 kDa) of Phe-PEA were opted and evaluated in detail. The high MW polymeric NPs exhibited higher loading capacity and higher stability than the low MW polymeric NPs. Although there was no significant difference in cellular uptake between these two types of NPs, the high MW polymeric NPs exhibited better anticancer efficacy against lymphoma *in vitro* and *in vivo* than DOX and the low MW polymeric NPs (Scheme 1).

The Phe-PEA polymers were synthesized through three steps previously reported [30,31]: (1) the synthesis of di-*p*-nitrophenyl ester of dicarboxylic acid (monomer I, denoted as "Nx," where "x" indicates the number of methylene groups in dicarboxylic acid), (2) the synthesis of tetra-*p*-toluenesulfonic acid salts of bis(L-Phe)-diester (monomer II, denoted as "Phe-y," where "y" indicates the number of methylene groups in diol), and (3) the synthesis of Phe-PEA polymers (denoted as "xpy") through polycondensation of monomers I and II. Details of the synthesis were applied in Supporting information. Different reaction time, temperatures and molar ratios were used to prepare different MW Phe-PEA polymers.

The chemical structures of the Phe-PEA polymers were examined *via* ^{1}H NMR spectroscopy (Bruker Avance III, Germany) and Fourier transform infrared (FTIR) spectroscopy (Bruker, Germany). The thermodynamic properties were investigated using differential scanning calorimetry (DSC, NETZSCH, Germany), and the MWs were measured *via* gel permeation chromatography (Agilent, USA) with a tetrahydrofuran column.

The nanoprecipitation method was used to prepare the Phe-PEA-based NPs owing to the hydrophobic properties of the Phe-PEA polymers. The polymer and DOX or dyes were dissolved in a 10 mg/mL dimethyl sulfoxide (DMSO) solution, and then DSPE-PEG2k was mixed with them as a stabilizer at a prearranged ratio. Then, the mixture was added dropwise to water under stirring to synthesize Phe-PEA-based NPs. The formulation was centrifuged and ultrafiltered using an ultrafiltration tube (100 kDa) to remove DMSO and concentrate it. Finally, the NPs were prepared in a 1× phosphate-buffered saline (PBS) solution for later use. Dynamic light scattering (DLS, Malvern Zatasizer, UK) was employed to measure the size distributions and zeta potentials of Phe-PEA-based NPs. The NP solution was dropped onto the carbon support film, and the morphology of the NPs was observed *via* transmission electron microscopy (TEM, JEOL, Japan) after natural drying. The stability of the Phe-PEA-based NPs was determined by analyzing the sizes of the NPs in PBS (pH 7.4) over a 7-d period. A microplate reader (BioTek, USA) was used to evaluate the loading capacities and encapsulation efficacies of DOX-loaded Phe-PEA NPs.

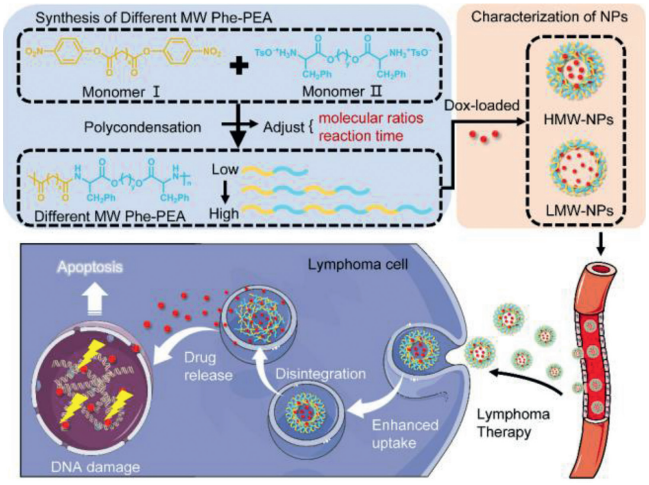

Scheme 1. Illustration of the DOX-loaded nanoplatform based on Phe-PEA polymers with different MWs for lymphoma therapy.

The drug-release behavior of DOX@Phe-PEA NPs was determined *via* the dialysis method as follows: 1 mL of NP solution was added to a dialysis bag (MWCO: 3500 Da) and then transferred to 10 mL of release buffer with different pH values, *i.e.*, 7.4 and 5.0, which were used to simulate the normal physiological environment and the microenvironment of the lysosome, respectively. The released samples were placed in a constant-temperature shaker at 37 °C and 100 rpm. At predetermined time intervals, 600 μL of the release medium was withdrawn and supplemented with an equal volume of fresh release medium. Finally, the amount of drug in the release medium was measured using a microplate reader.

The cytotoxicity of Phe-PEA-based NPs in A20 cells was investigated using the CKK-8 assay. The procedure was as follows. A20 cells at the logarithmic growth stage were incubated at a density of 8000 cells/well and cultured overnight at 37 °C in a humidified atmosphere containing 5% CO_2. Then, 100 μL of a medium containing Phe-PEA NPs, DOX, or DOX@Phe-PEA NPs at different concentrations was added to each well. The cells incubated with the culture medium were considered as negative control samples, and the cell-free wells were considered as blank samples. After 24 h of incubation, 10 μL of CKK-8 reagent was added to each well, followed by 2 h of incubation. Finally, the absorbance of each well in different groups at 450 nm was measured using a BioTek microplate reader. The cell viability of each group was calculated according to the relative absorbance, using the following equation:

$$\text{Cell viability}\,\% = \left(\text{Ab}_{\text{sample}} - \text{Ab}_{\text{blank}}\right)/\left(\text{Ab}_{\text{control}} - \text{Ab}_{\text{blank}}\right) \times 100\%$$

The cell apoptosis in A20 cells was detected *via* flow cytometry (SP6800, Sony, Japan), as follows. A20 cells were seeded at a density of 2×10^5 cells/well and cultured at 37 °C in a humidified atmosphere containing 5% CO_2 overnight. Then, the medium was discarded, and a medium containing Phe-PEA NPs, DOX (0.5 μg/mL), or DOX@Phe-PEA NPs (with 0.5 μg/mL DOX) was added. Cells treated with the culture medium were used as controls. After 24 h of incubation, the medium was discarded *via* centrifugation and washed twice with PBS, and the cells were resuspended in 500 μL of an Annexin V-APC/7AAD working solution and maintained for 15 min in the dark. Finally, the cells were analyzed for apoptosis using flow cytometry.

The uptake of DOX@Phe-PEA NPs by A20 cells was investigated using flow cytometry, as follows. A20 cells were incubated in six-well plates at a density of 2×10^5 cells/well and cultured overnight. Then, the medium containing free DOX (0.2 μg/mL) or DOX@Phe-PEA NPs (0.2 μg/mL DOX) was added and incubated with the A20 cells for 0.5, 1, 4, and 6 h. Next, the medium was discarded *via* centrifugation, the cells were washed three times with PBS, and flow cytometry was used for fluorescence quantification.

Confocal laser scanning microscopy (CLSM, Zeiss, Germany) was used to observe the lysosomal escape of DOX@Phe-PEA NPs in A20 cells. Similar to the previous step, A20 cells were incubated overnight, and DOX@Phe-PEA NPs with a DOX concentration of 0.4 μg/mL were then incubated with the cells for 1 and 4 h. After centrifugation and washing, 1 mL of the nuclear dye Hoechst 33,342 (5 μg/mL) and 1 mL of the lysosomal dye LysoTracker Green (75 nmol/L) were added, followed by incubation for 10 and 30 min, respectively. The cells were then washed and dispersed in PBS. Finally, the cells were transferred to a confocal dish and photographed using CLSM.

All animal experiments were conducted in accordance with the guidelines of the Institutional Animal Care and Use Commit-

tee of Sun Yat-sen University. A fluorescent dye 1,1-dioctadecyl-3,3,3,3-tetramethylindotricarbocyaineiodide (DiR) was selected to label NPs *in vivo*. DiR@Phe-PEA NPs were prepared according to the same nanoprecipitation method as DOX@Phe-PEA NP preparation, and the biodistribution of the NPs in A20 tumor-bearing nude mice was studied using an *in vivo* imaging system (IVIS, PerkinElmer, USA). Briefly, A20 tumor-bearing nude mice were randomly divided into two groups and injected intravenously with DiR@4P4-L NPs (0.5 mg/kg DiR) and DiR@4P4-H NP solution (0.5 mg/kg DiR), respectively. At predetermined time points, the mice were anesthetized, and fluorescence images were obtained using IVIS. Twenty four hours after the injection, the mice were euthanized, and the major organs (heart, lung, spleen, liver, and kidney) and tumor tissues were excised for fluorescence imaging. The tumor tissues of both groups were frozen, sectioned, and stained with FITC/Anti-CD31 antibody (to label the blood vessels) and 4′,6-diamidino-2-phenylindole (DAPI) (to label the nuclei) for observing the biodistribution and deep penetration of NPs in tumor sites *via* fluorescence microscopy.

An A20-tumor bearing mouse model was used to verify the therapeutic effect of DOX@Phe-PEA NPs on lymphoma. First, 100 μL of A20 cell suspension was subcutaneously injected into the backs of BALB/c nu/nu mice at a density of 3×10^7 cells per mouse to construct a subcutaneous transplantation tumor model. When the tumor volume reached approximately 50–100 mm^3, the mice were randomly divided into six groups and treated with tail vein injection of the following formulations: saline (control group), 4P4-L NPs, 4P4-H NPs, DOX (5 mg/kg), DOX@4P4-L NPs (5 mg/kg DOX), and DOX@4P4-H NPs (5 mg/kg DOX). During the treatment period, the formulations were injected every 2 d for a total of five injections, and the body weight and tumor volume of each mouse were recorded once per day. At the end of the treatment, serum was collected for evaluating blood biochemical parameters, including aspartate aminotransferase (AST), alkaline phosphatase (ALP), alanine aminotransferase (ALT), blood urea nitrogen (BUN), creatinine (CRE), and kinase (CK). The mice were euthanized, their tumors were photographed and weighed, and the tumor sections were fixed in 4% paraformaldehyde (PFA) for H&E section staining and a TUNEL apoptosis assay. The primary organs of the mice in each group (heart, lung, spleen, liver, and kidney) were collected and fixed in 4% PFA for H&E section analysis.

To develop Phe-PEA, two monomers were employed for normal solution polycondensation, as previously reported (Fig. 1A). The Phe-PEA was denoted as “xPy,” where “x” indicates the number of methylene groups in monomer I, and “y” indicates the number of methylene groups in monomer II. To obtain Phe-PEA with different MWs, the molar ratio of the monomers and reaction time were finely tuned. As shown in Fig. 1B, for the 4P4 system, with

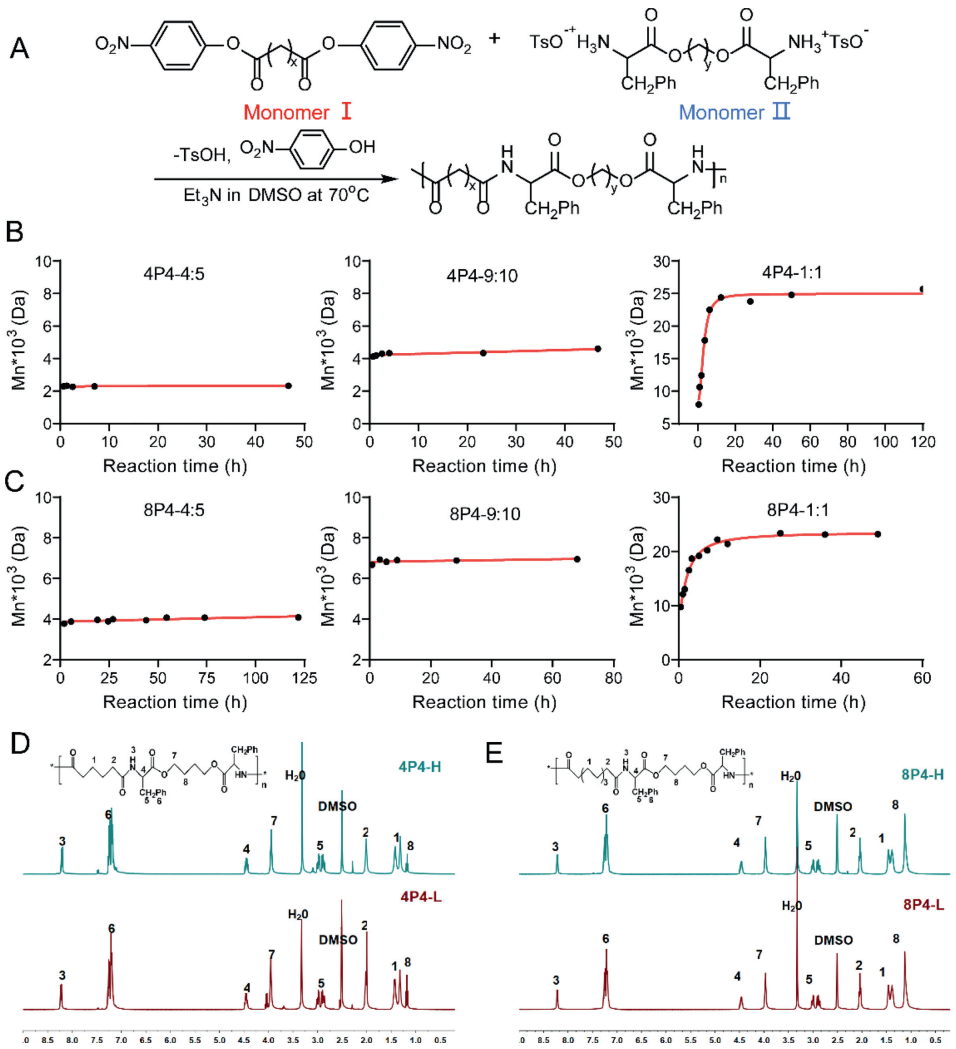

Fig. 1. (A) Synthetic route for the Phe-PEA polymers. (B) Effects of the molar ratio and reaction time on the MW of 4P4. (C) Effects of the molar ratio and reaction time on the MW of 8P4. (D) ^{1}H NMR spectra of 4P4-L and 4P4-H polymers. (E) ^{1}H NMR spectra of 8P4-L and 8P4-H polymers.

$r = 0.8$, the MW of 4P4 reached approximately 2.3k quickly and remained constant thereafter; with $r = 0.9$, the MW of 4P4 reached approximately 4.6k very quickly and remained constant thereafter; with $r = 1.0$, the MW of 4P4 increased quickly in the first 10 h and then remained constant (above 20k). Similar results are observed in Fig. 1C: for the 8P4 system, with $r = 0.8$, the MW of 8P4 reached approximately 4k very quickly and remained constant thereafter; with $r = 0.9$, the MW of 8P4 reached approximately 7k very quickly and remained constant thereafter; with $r = 1.0$, the MW of 8P4 increased quickly in the first 10 h and then remained constant (above 20k). For saturated PEA ($r = 1$), the polymerization process could be roughly divided into three stages: 0–5 h (fast growth), 5–12 h (slow growth), and 12 h (steady growth). A slow or steady growth indicates that the activity of the PEA (the activity of the end group) is low or dead. For the fast stage, 0–0.5 h was the most uncontrollable part, and 0.5–5 h was comparatively controllable (Figs. 1B and C)

To evaluate the effects of the MW on the physicochemical properties of Phe-PEA and the corresponding polymeric NPs, two types of Phe-PEA with large MW differences were selected. A ratio of 4:5 was used for the synthesis of low-MW Phe-PEA (4P4-L and 8P4-L), and the high-MW Phe-PEA (4P4-H and 8P4-H) was synthesized at a ratio of 1:1 (Table S1 in Supporting information). The chemical structures of the Phe-PEA with different MWs were confirmed by ^{1}H NMR and FTIR spectroscopy, as shown in Fig. S1 (Supporting information). The proton peak of the amide bond was observed at 8.25 ppm, indicating successful polymerization (Figs. S1D and E). The C=O stretching peaks at 1720 and 1670 cm^{-1} confirmed the successful polymerization (Fig. S1A). There were no differences in the ^{1}H NMR or FTIR spectra between the high-MW and low-MW Phe-PEA polymers. The thermodynamic properties of the Phe-PEA were evaluated using DSC. As indicated by Fig. S1B and Table S1, the glass transition temperature (T_g) and thermal property differences between the high-MW and low-MW Phe-PEA were small.

DOX, a standard clinical chemotherapeutic for lymphoma therapy, was selected as a model drug to evaluate the effect of the MW on the properties of the Phe-PEA-based NPs, such as their loading capacities and drug-release profiles. First, a series of drug-loaded NPs were prepared by encapsulating DOX into Phe-PEA polymers *via* nanoprecipitation, and then the particle sizes and particle-size distributions of the Phe-PEA-based NPs were measured *via* DLS. As indicated by Figs. 2D and E and Table S2 (Supporting information), the blank carrier NPs exhibited a narrow particle-size distribution in the range of 60–90 nm, the PDI distribution was between 0.11 and 0.15, and the zeta potential was close to neutral. Compared with the blank carrier NPs, the particle size of drug-loaded NPs changed slightly, except for the DOX@8P4-L NPs, which had a significantly increased particle size. The TEM images of the NPs indicated that both types of NPs had a well-defined spherical structure, which was consistent with the DLS results (Figs. 2F and G and Table S2).

Next, different DOX@Phe-PEA NPs were dispersed in PBS (pH 7.4), and their sizes were monitored for 7 d to evaluate their stability in a physiological environment. As shown in Fig. 2A, the particle size of the high-MW DOX-loaded NPs was slightly changed after 7 d, indicating good stability. However, the particle size of the low-MW DOX@Phe-PEA NPs increased from 74 nm to 145 nm (4P4-L) and from 139 nm to 182 nm (8P4-L) in the first 4 d and remained stable for the last 3 d, indicating that a low MW would affect the stability of the corresponding polymeric NPs. A similar phenomenon was observed in the evaluation of the drug loading capacity. The high-MW DOX@Phe-PEA NPs exhibited a better DLC, *i.e.*, 8.44% ± 0.15% (4P4-H) and 9.49% ± 0.16% (8P4-H), than the low-MW DOX-loaded NPs, which indicated that as the polymer

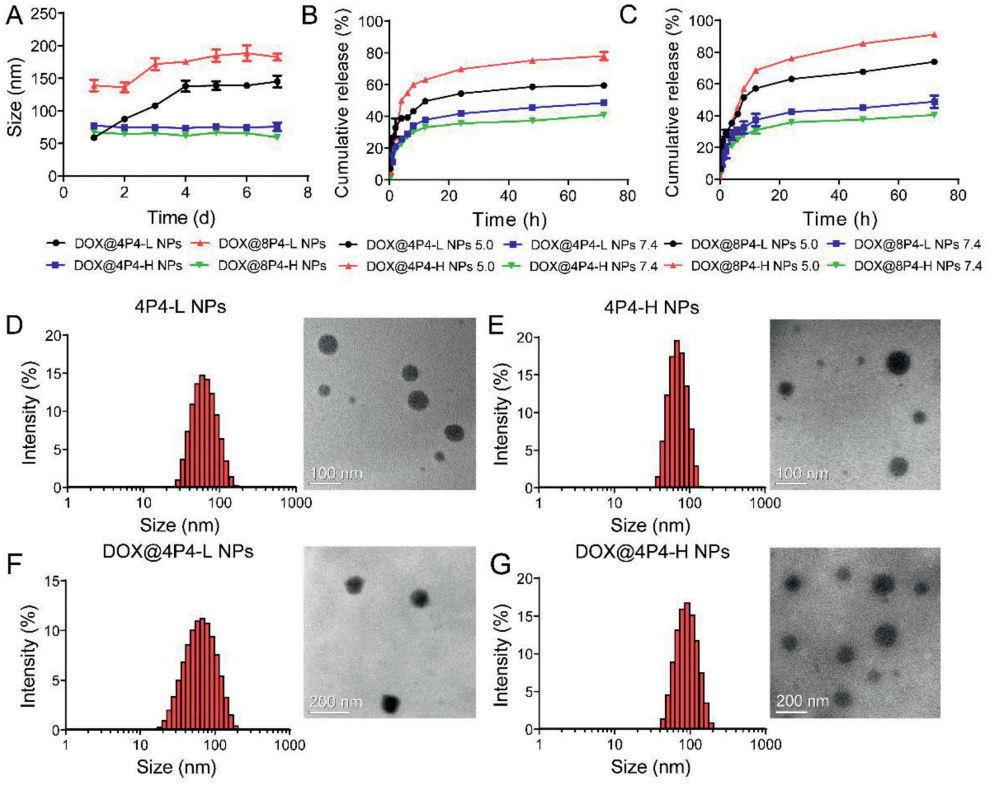

Fig. 2. (A) Stability of DTX@Phe-PEA NPs in PBS for 7 d. (B) *In vitro* DOX release from DOX@4P4-L NPs and DOX@4P4-H NPs under different pH conditions. (C) *In vitro* DOX release from DOX@8P4-L NPs and DOX@8P4-H NPs under different pH conditions. Size distribution (left) and TEM images (right) of 4P4-L NPs (D), 4P4-L NPs (E), DOX@4P4-L NPs (F) and DOX@4P4-H NPs (G).

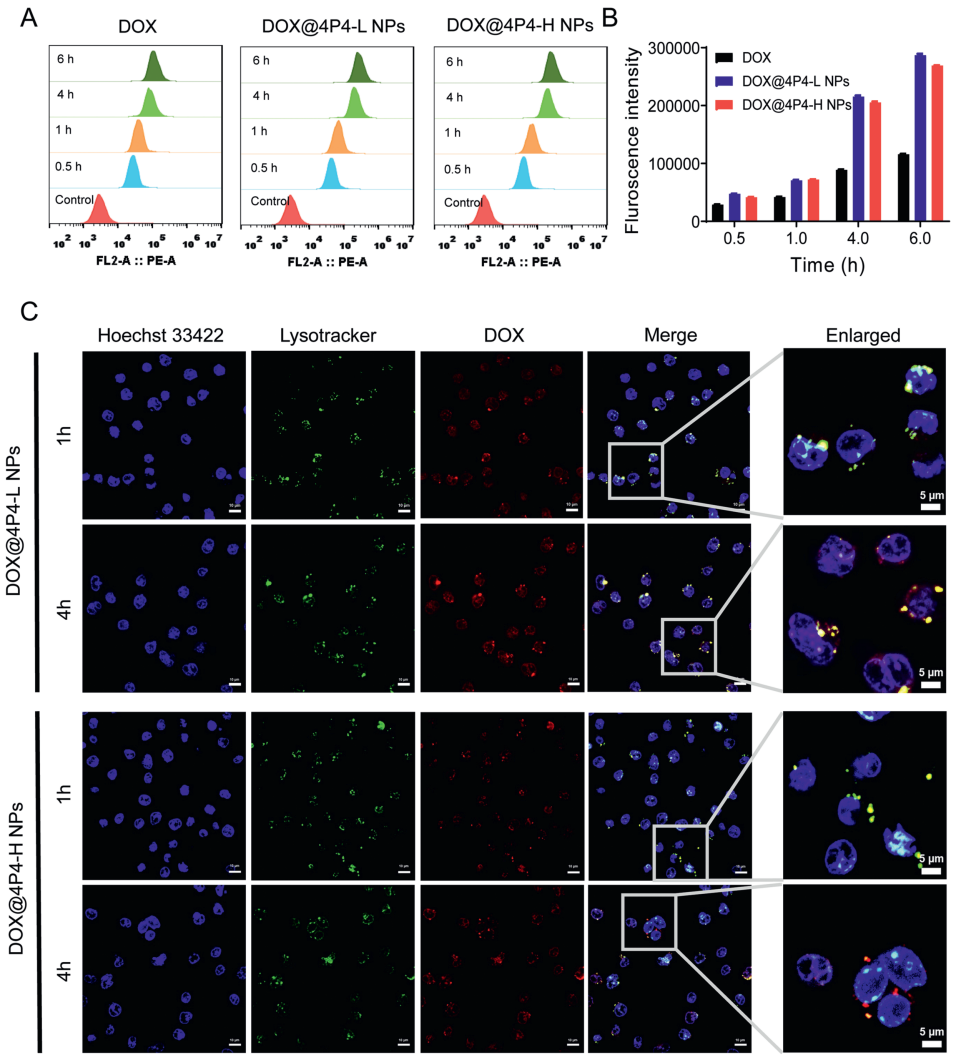

Fig. 3. (A) Fluorescence histograms of the A20 cells incubated with free DOX, DOX@4P4-L NPs and DOX@4P4-H NPs. (B) Mean fluorescence intensity of DOX, DOX@4P4-L NPs and DOX@4P4-H NPs internalized by A20 cells for 0.5, 1, 4, and 6 h. (C) Confocal microscopy images of A20 cells incubated with DOX@4P4-L NPs and DOX@4P4-H NPs for 1 and 4 h (scale bar = 10 μm, enlarged scale bar = 5 μm).

MW increased, the drug loading efficiency of the Phe-PEA polymer was improved. These results suggest that high-MW Phe-PEA NPs are a promising drug-delivery system for cancer therapy.

The drug-release profiles were obtained using the dialysis method, and the release buffers were PBS with pH values of 7.4 (physiological condition) and 5.0 (acidic tumor microenvironment). As shown in Figs. 2B and C, the release rates of all the DOX@Phe-PEA NPs in the PBS solution at the pH of 7.4 were low, and the final cumulative drug release was <45%. In comparison, in the acidic environment (pH of 5.0), the release rate of the drug was higher, the final cumulative drug release was significantly enhanced, and the cumulative release of high-MW DOX@Phe-PEA NPs exceeded that of low-MW DOX@Phe-PEA NPs. These results indicated that the acidic environment promoted the drug release from the DOX@Phe-PEA NPs. It can be inferred that the high-MW DOX@Phe-PEA NPs can enhance drug release at the tumor site, which would have beneficial anticancer effects.

Cellular uptake efficiency is critical for evaluating NP function. In this study, flow cytometry was used to quantify the uptake of DOX@Phe-PEA NPs by A20 cells. As shown in Fig. 3A, A20 cells exhibited significantly enhanced red fluorescence after incubation with DOX@Phe-PEA NPs, and the fluorescence intensity increased with the incubation duration. These results indicated that the DOX@Phe-PEA NPs were rapidly and effectively taken up by tumor cells, and the uptake efficiency was higher than that of free DOX (Fig. 3B). Thus, the DOX@Phe-PEA NPs with both MWs promoted efficient drug uptake by A20 tumor cells.

Next, CLSM was used to determine whether the DOX@Phe-PEA NPs could escape from the lysosomes of A20 cells. As shown in Fig. 3C, after 1 h of incubation with DOX@Phe-PEA NPs, the red fluorescence of the NPs mostly overlapped with the green fluorescence of the lysosomes, resulting in yellow fluorescence, which indicates that the NPs were mainly distributed in lysosomes at 1 h. With the incubation time increased to 4 h, the green fluorescence was separated from the red fluorescence, and the yellow fluorescence was significantly reduced, indicating that the DOX@Phe-PEA NPs successfully escaped from the lysosomes into the cytoplasm. In summary, DOX@Phe-PEA NPs enhanced the cellular uptake and achieved lysosomal escape in both high and low DOX-loaded NPs.

Encouraged by the cellular uptake results, the *in vitro* cytotoxicity of DOX and DOX@Phe-PEA NPs in A20 cells was assessed using the CKK-8 method. As shown in Fig. 4A, after incubation with different concentrations of Phe-PEA NPs, the viability of A20 cells was not significantly reduced and remained at approximately 90%. However, the viability of A20 cells was significantly reduced after treatment with different concentrations of free

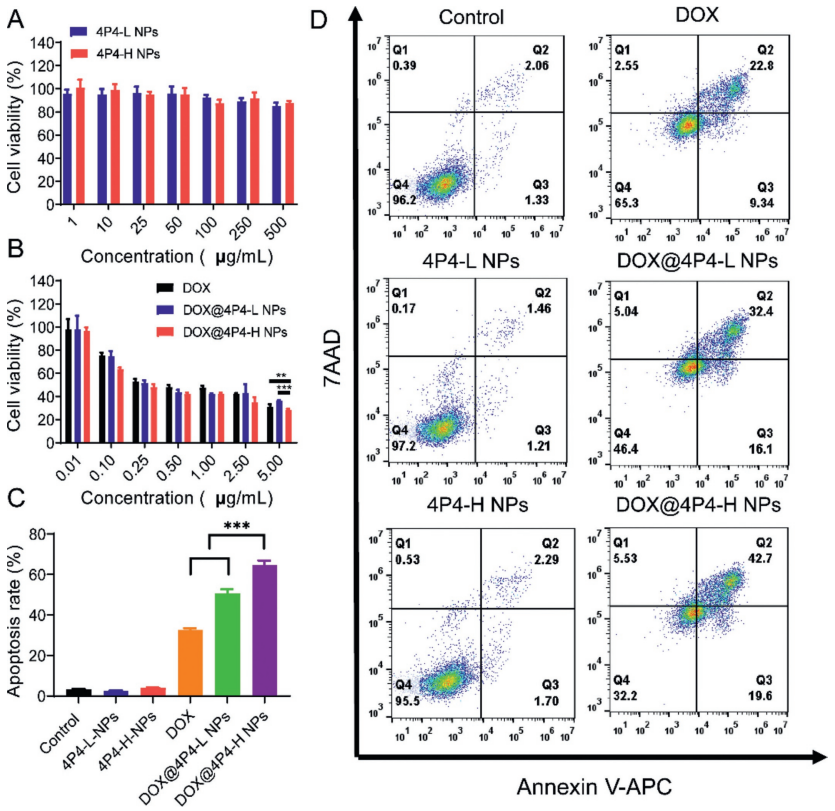

Fig. 4. (A) *In vitro* cytotoxicity of A20 cells treated with Phe-PEA NPs at different concentrations for 24 h. (B) *In vitro* cytotoxicity of A20 cells treated with DOX and DOX@Phe-PEA NPs at different concentrations for 24 h. (C) *In vitro* apoptotic rates of A20 cells treated with Phe-PEA NPs, DOX and DOX@Phe-PEA NPs for 24 h. (D) Cell apoptosis of A20 cells incubated with Phe-PEA NPs, DOX and DOX@Phe-PEA NPs measured by a flow cytometer. $^{**}P < 0.01$, $^{***}P < 0.001$.

DOX and DOX@Phe-PEA NPs for 24 h, and the reduction was dose-dependent (Fig. 4B). The semi-inhibitory concentrations (IC_{50}) of DOX, DOX@4P4-L NPs, and DOX@4P4-H NPs were 0.74, 0.66, and 0.41 μg/mL, respectively. These results may be due to the instability and less drug release amount of DOX@4P4-L NPs which finally lead to lower cytotoxicity. Thus, it was concluded that DOX@4P4-H NPs had a better cytotoxic effect on A20 cells than free DOX and DOX@4P4-L NPs.

To further investigate the induction of apoptosis by DOX@Phe-PEA NPs, A20 cells were treated with Phe-PEA NPs, DOX, and DOX@Phe-PEA for 24 h. Apoptotic cells were labeled with Annexin V-APC/7AAD and subjected to flow cytometry. As shown in Figs. 4C and D, the apoptosis in the Phe-PEA NP group was comparable to that in the control group, indicating that Phe-PEA NPs do not induce apoptosis and have good biocompatibility. In contrast, after 24 h of treatment with DOX and DOX@Phe-PEA, A20 cells exhibited significant apoptosis, with apoptotic rates of 32.63% ± 0.84% (DOX), 50.60% ± 2.00% (DOX@4P4-L NPs), and 62.77% ± 2.14% (DOX@4P4-H NPs). Thus, it is evident that high-MW NPs can enhance the *in vitro* antitumor activity of DOX.

It is widely known that NPs of specific sizes can be passively targeted to tumor sites through the enhanced permeability and retention (EPR) effect, extending the *in vivo* circulation time. To investigate the targeting of DOX@Phe-PEA NPs in A20 xenograft-bearing mice, DiR was selected to mimic the drug and label the NPs, and fluorescence imaging of the mice was performed by IVIS after DiR-loaded NPs were injected into the mice *via* the tail. As shown in Fig. 5A, 1 h after injection, the NPs rapidly aggregated at the tumor site. The fluorescence intensity of the DiR-loaded NPs at the tumor site increased over time and reached its maximum value at 12 h. In addition, the images of *ex vivo* major organs in Fig. 5B and the quantitative analysis results in Fig. 5C confirmed that the

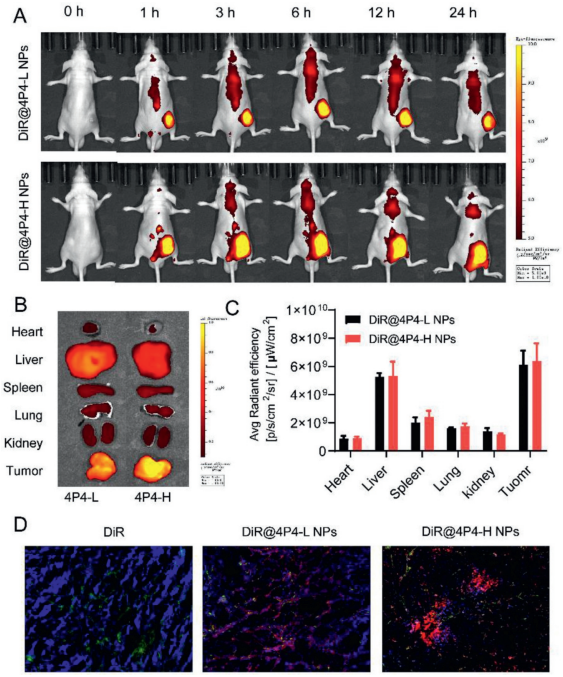

Fig. 5. (A) DiR fluorescence images of Phe-PEA NPs with different MWs distributed in mice at different times after intravenous injection. (B) DiR fluorescence images of the *ex vivo* biodistribution of Phe-PEA NPs with different MWs. (C) Quantitative results for the fluorescence intensity in major organs and tumor accumulation. (D) Fluorescence images of Phe-PEA NPs with different MWs distributed in tumor sections. Green fluorescence corresponds to CD31, indicating blood vessels; blue fluorescence corresponds to DAPI, indicating nuclei; and red fluorescence corresponds to DiR, indicating NPs (scale bar = 100 μm).

DiR-loaded NPs enhanced the tumor accumulation compared with other major organs. However, there was no significant difference between the NPs with different MWs. The results indicated that DiR-loaded NPs with suitable particle sizes can be rapidly and effectively targeted to lymphoma tissues, can enhance the accumulation of drugs in tumor tissues, and can prolong retention in tumor tissues.

To further investigate the penetration of NPs into the A20 tumor site, the tumor sections were stained with Anti-CD31 monoclonal antibody for labeling tumor blood vessels with green fluorescence, DAPI for labeling cell nuclei with blue fluorescence, and DIR for labeling NPs with red fluorescence. As shown in Fig. 5D, red fluorescence was hardly detected in the tumor sites of DiR-treated mice, implying that free DiR had difficulty aggregating at the tumor sites. In contrast, the red fluorescence signal of the DiR-loaded NPs at the tumor sites was significant. The red fluorescence of DiR@4P4-L NPs overlapped with the green fluorescence of the blood vessels (Fig. 5D); however, the red fluorescence of DiR@4P4-H NPs could aggregate far from the green vessels (Fig. 5D), confirming that the DiR@4P4-H NPs penetrated the tumor blood vessels, entering the tumor interstices. Deep tumor penetration and accumulation allow DOX-loaded NPs to exert their antitumor effects.

Encouraged by the efficient cellular uptake, enhanced cytotoxicity, cell apoptosis, deep tumor penetration, and accumulation of NPs, an A20 tumor-bearing mouse model was used to verify the *in vivo* antitumor effects of DOX@Phe-PEA NPs. Within the treatment duration, the body weight and tumor volume of the mice were recorded daily, the tumor growth curves were plotted, and the tumors were photographed and weighed at the end of the treatment to assess the tumor suppression effect. After treatment with the different formulations, the tumors in the mice exhibited different growth trends. For the negative control and Phe-PEA NP treatment groups, the tumors grew rapidly with the same trend, and the tumor volumes reached $>1500\,mm^3$ after 12 d of treatment. However, the tumor growth was inhibited in mice treated with free DOX and DOX@Phe-PEA NPs, and the tumor inhibition rates were 54.4% and 67.0% (DOX@4P4-L NPs) and 76.5% (DOX@4P4-H NPs), respectively (Figs. 6A and C). Meanwhile, there was no obvious weight loss in each group (Fig. 6B). The tumors were excised and weighed at the end of the treatment, which revealed similar trends in the tumor volume growth and imaging results (Fig. 6D). Thus, the high-MW DOX@Phe-PEA NPs exhibited better antitumor efficacy than the DOX-treated and low-MW DOX@Phe-PEA NP groups. In addition, there were no significant changes in the body weights of the mice in any of the groups during the entire treatment pe-

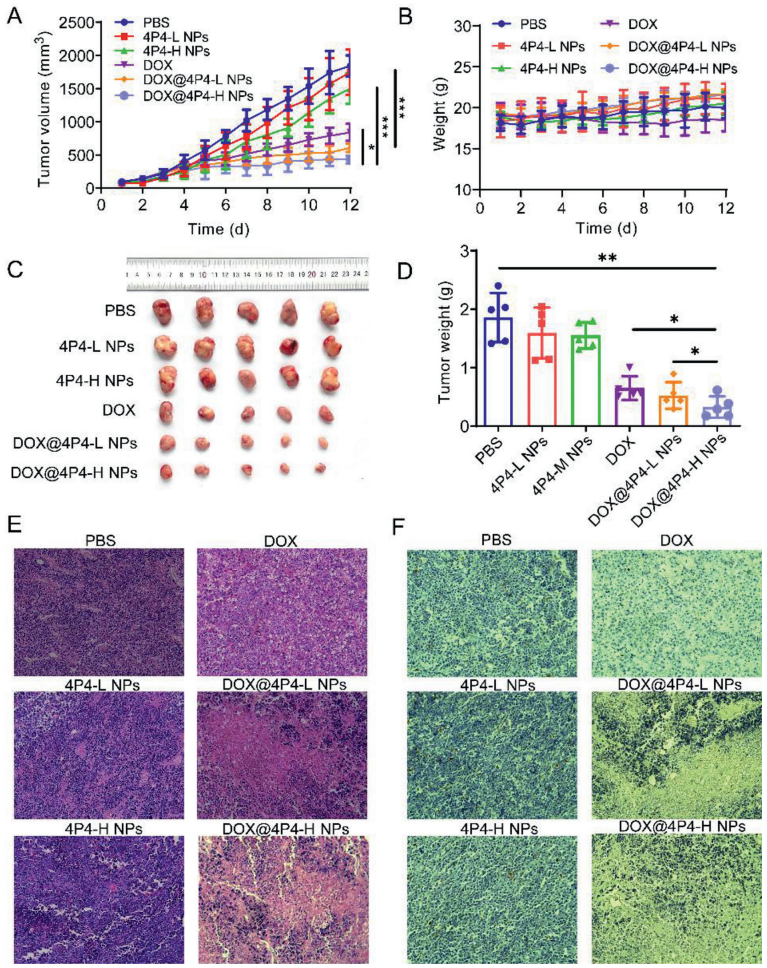

Fig. 6. (A) Tumor growth inhibition of A20 tumor-bearing mice after intravenous injection with PBS, Phe-PEA NPs, DOX and DOX@Phe-PEA NPs. (B) Body weights of A20 tumor-bearing mice after intravenous injection with different formulations over the treatment. (C) Representative image of a extracted tumor from an A20 tumor-bearing mouse after treatment. (D) Weights of dissected tumors from mice after treatment. (E) H&E and (F) TUNEL staining images of tumor sections for cell apoptosis analysis after treatment with different formulations (scale bar = 100 μm). $^{*}P < 0.05$, $^{**}P < 0.01$, $^{***}P < 0.001$.

riod, confirming that the treatments did not cause serious toxic side effects in the mice.

To further investigate the antitumor effect, H&E and TUNEL staining of tumor sections were performed for evaluation at the end of the treatment. As shown in Figs. 6E and F, for the control and Phe-PEA NP groups, the tumor sections were structurally intact and tight, and no obvious nuclear abnormalities were observed. In contrast, for the DOX and DOX@Phe-PEA NP groups, the tumor tissues were loosely structured and exhibited obvious nuclear crinkling and fragmentation, indicating that the tumor tissues underwent severe apoptosis and necrosis; the apoptotic necrosis of the tumor cells in the DOX@Phe-PEA NP group was more serious. These results confirmed the superior antitumor effect of the DOX@Phe-PEA NPs.

To assess the *in vivo* safety of DOX@Phe-PEA NPs, blood and major organs were separated from the mice at the end of the treatment for blood biochemical analysis and histological analysis. The blood biochemical test indices included liver function indices such as AST, ALT, and ALP; renal function indices such as BUN and CRE; and the cardiac enzyme index CK. As shown in Fig. S2 (Supporting information), there were no significant differences in any of the groups, confirming that the carrier materials and drug-loaded NPs did not have significant toxic side effects on the liver, kidney, or heart and had a good safety profile. In addition, as shown in Fig. S3 (Supporting information), the H&E staining results revealed no significant organic changes or inflammatory damage in the mice after multiple treatments, which confirmed the *in vivo* safety of the vector and drug-loaded DOX@Phe-PEA NPs.

To investigate the effects of the polymer MW on drug delivery and lymphoma therapy, we synthesized a series of Phe-PEA polymers with different MWs by varying the monomer ratio and reaction time. The high-MW polymer-based NPs exhibited a higher loading capacity of DOX and higher stability than the low-MW polymer-based NPs. Moreover, *in vitro* and *in vivo* data indicated that the high-MW polymeric NPs had better anticancer efficacy against lymphoma and deep tumor penetration than the low-MW polymeric NPs and DOX. Therefore, this study highlights the importance of the polymer MW for drug-delivery systems and provides a basis for the design of enhanced polymeric drug-delivery systems for lymphoma therapy.

Declaration of competing interest

The authors declare that they have no known competing financial interests or personal relationships that could have appeared to influence the work reported in this paper.

Acknowledgments

This work was supported by the National Natural Science Foundation of China (Nos. 51973243 and 52173150), International Cooperation and Exchange of the National Natural Science Foundation of China (No. 51820105004), China Postdoctoral Science Foundation (No. 2020M683058), Shenzhen Science and Technology Program (No. RCBS20210706092411033), the Science and Technology Planning Project of Shenzhen (No. JCYJ20190807155801657), Guangdong Innovative and Entrepreneurial Research Team Program (No. 2016ZT06S029).

Supplementary materials

Supplementary material associated with this article can be found, in the online version, at doi:10.1016/j.cclet.2022.07.063.

References

[1] H. Sung, J. Ferlay, R.L. Siegel, et al., CA A Cancer J. Clin. 71 (2021) 209–249.
[2] J.S. O'Donnell, E.P. Hoefsmit, M.J. Smyth, C.U. Blank, M.W.L. Teng, Clin. Cancer Res. 25 (2019) 5743–5751.
[3] S.P. Pitroda, S.J. Chmura, R.R. Weichselbaum, Lancet Oncol. 20 (2019) e434–e442.
[4] G. Bocci, R.S. Kerbel, Nat. Rev. Clin. Oncol. 13 (2016) 659–673.
[5] V.T. DeVita, E. Chu, Cancer Res. 68 (2008) 8643.
[6] S. Mitragotri, P.A. Burke, R. Langer, Nat. Rev. Drug Discov. 13 (2014) 655.
[7] T. Souho, L. Lamboni, L. Xiao, G. Yang, Biotechnol. Adv. 36 (2018) 1928–1945.
[8] I. de Lazaro, D.J. Mooney, Nat. Mater. 20 (2021) 1469–1479.
[9] L. Fang, Z. Zhao, J. Wang, et al., Acta Pharm. Sin. B B 12 (2022) 353–363.
[10] Y. Qu, B. Chu, X. Wei, et al., J. Control. Release 296 (2019) 93–106.
[11] M. Elsabahy, G.S. Heo, S.M. Lim, G. Sun, K.L. Wooley, Chem. Rev. 115 (2015) 10967–11011.
[12] X. You, Y. Kang, G. Hollett, et al., J. Mater. Chem. B 4 (2016) 7779–7792.
[13] Y. Cui, T. Zhu, X. Zhang, et al., Chin. Chem. Lett. 33 (2022) 4617–4622.
[14] B. Chu, Y. Qu, X. He, et al., Adv. Funct. Mater. 30 (2020) 2005918.
[15] H. Guo, F. Li, H. Qiu, et al., Research 2020 (2020) 8970135.
[16] Z. Zhao, A. Ukidve, V. Krishnan, S. Mitragotri, Adv. Drug Deliv. Rev. 143 (2019) 3–21.
[17] A. Bernkop-Schnürch, Adv. Drug Deliv. Rev. 136-137 (2018) 62–72.
[18] X. Zheng, J. Xie, X. Zhang, et al., Chin. Chem. Lett. 32 (2021) 243–257.
[19] N. Kamaly, B. Yameen, J. Wu, O.C. Farokhzad, Chem. Rev. 116 (2016) 2602–2663.
[20] Y. Wang, J. Wang, D. Zhu, et al., Acta Pharm. Sin. B 11 (2021) 886–902.
[21] S. Arpicco, M. Bartkowski, A. Barge, et al., Front. Chem. 8 (2020) 578008.
[22] J.E. Dahlman, C. Barnes, O.F. Khan, et al., Nat. Nanotechnol. 9 (2014) 648–655.
[23] M.M. Abdelghafour, Á. Orbán, Á. Deák, et al., Int. J. Pharm. 618 (2022) 121653.
[24] G. Li, S. He, A.G. Schätzlein, et al., J. Control. Release 332 (2021) 210–224.
[25] U. Capasso Palmiero, M. Maraldi, N. Manfredini, D. Moscatelli, Biomacromolecules 19 (2018) 1314–1323.
[26] H. Liu, S.S. Venkatraman, J. Pharm. Sci. 103 (2014) 485–495.
[27] D. Lou, X. Lu, M. Zhang, M. Bai, J. Jiang, Chem. Commun. 54 (2018) 6987–6990.
[28] X. You, Z. Gu, J. Huang, et al., Acta Biomater. 74 (2018) 180–191.
[29] M. Rhee, P.M. Valencia, M.I. Rodriguez, et al., Adv. Mater. 23 (2011) H79–H83.
[30] J. Wu, C.C. Chu, J. Mater. Chem. B 1 (2013) 353–360.
[31] J. Wu, C.C. Chu, Acta Biomater. 8 (2012) 4314–4323.